PHYSICAL REVIEW B VOLUME 36, NUMBER 12 15 OCTOBER 1987-II

New classical models for silicon structural energies

R. Biswas* and D. R. Hamann
AT&T Bell Laboratories, Murray Hill, New Jersey 07974-2070
(Received 2 February 1987)

A theory of classical two- and three-body interatomic potentials is developed. The ability of the classical potentials to model quantum-mechanical local-density-functional calculations for a wide range of silicon structures is explored. In developing classical models it was found to be necessary to perform new local-density-functional calculations for self-interstitial and layered silicon structures. Two different potentials are derived from fits and tests to energies of bulk, surface, layered, and self-interstitial structures. One potential models bulk energies and high-pressure properties well; the other is more appropriate for properties of the tetrahedral structure. Simulated annealing is used to find low-energy structures for silicon-atom clusters.

I. INTRODUCTION

An understanding of the structure and properties of materials from a microscopic level is an area of much current interest. Quantum-mechanical calculations, particularly with the local-density-functional approach, have been extremely successful in predicting properties of simple structures. However, these methods are presently limited to high-symmetry structures with at most a few tens of atoms per unit cell, and to exploring a very limited part of configuration space. For molecular dynamics simulations or global searches for energy minima of larger systems, only classical interatomic force fields are practical. Systems where such classical methods may be most fruitful include studies of melting, crystal growth, epitaxy, amorphous structures, and atomic clusters.

With a view to developing new methods to deal with such applications, we develop in this paper a general theory of two- and three-body interatomic potentials for modeling structural energies of solids. Pair potentials have been extensively used to model rare-gas solids and simple metals, but at least three-body interactions are necessary for strongly bonded systems. In fact, the three-body Keating model[1] which is fitted to small distortions of the diamond structure, has had much success in describing local distortions and phonons, but has also been extrapolated to compute energies of complex Si structures, sometimes beyond its range of validity. We explore here the feasibility of a global model of classical potentials. We confine our explorations to two- and three-body models, since the derivation of atomic forces becomes exceedingly complex for higher multiatom models, and this restricts their utility for molecular dynamics simulations. Silicon is the material of choice because of the large number of local-density approximation (LDA) structural energy calculations[2,3] for simple structures that span a wide range of atomic bonding geometries. In developing classical models for silicon, we found it necessary to perform further LDA calculations on self-interstitials and slabs of both diamond and metallic structures. Our LDA calculations are described in Sec. III and should be useful in developing and testing other classical models.

We have explored in this paper the ability of classical theories to model a wide variety of quantum-mechanical calculations. We highlight the strengths of such classical models and also identify their potential weaknesses. We have previously reported a classical two- and three-body Si potential.[4] We study this classical model in more detail here, and identify its deficiencies for layered and interstitial structures.

We then develop a new Si potential that improves considerably on the deficiencies of the former model. As a result though, the new potential does less well in describing bulk metallic Si structures, and the high-pressure transitions of Si, which the old potential modeled very well. The short range of the new model does, however, make it very attractive for molecular-dynamics simulations.

We note that the development of classical models for silicon has been an extremely active area. Pearson, Takai, Halicionglu, and Tiller (PTHT) (Ref. 5) have developed a nonseparable[4] three-body Si potential that is a generalization of the Axilrod-Teller three-body interaction.[6] This potential is long ranged (decaying as $1/r^9$). Stillinger and Weber[7] (SW) have developed a short-range model confined to two neighbor shells where the angular variation of the three-body potential has a Keating type of form. Recently, Tersoff[8] has developed a pair potential model of Si where the strength of the pair potential depends on the atomic bonding environment. This effectively couples three body and higher multiatom correlations into the model.

Our theory of the interatomic potentials is developed in Sec. II. Connections are drawn to the description of bond orientational order in liquids and to the embedded atom approach. Our LDA calculations of energies of Si structures are described in Sec. III. The ability of classical potentials to model these quantum-mechanical results is explored in Sec. IV, and a new Si potential is developed. Structural properties of atomic Si clusters from the new potential are described in Sec. V. Conclusions are summarized in Sec. VI.

II. CLASSICAL INTERATOMIC POTENTIAL MODELS—THEORY

Our two- and three-body potential model is defined by the following expression for the structural energy:

$$E=\tfrac{1}{2}\sum_{1,2}{}' V_2(1,2)+\sum_{1,2,3}{}' V_3(1,2,3)\ , \tag{1}$$

where primes indicate that all summation indices are distinct. There is no explicitly volume-dependent term, since atomic volume is not a useful physical concept for inhomogenous structures. The assumption of neglecting four-body and higher terms is used and tested in the present work. Any three-body potential $V_3(1,2,3)$ may be expressed as a function of two lengths r_{12},r_{13} and the included angle θ_1. This potential is symmetrized over the three particles in the sums in (1). Without losing generality we can expand the angular dependence of this potential in the complete set of Legendre polynomials. The coefficients in this expansion are functions F_l of bond lengths multiplied by linear coefficients C_l,

$$V_3(r_{12},r_{13},\theta_1)=\sum_l C_l F_l(r_{12},r_{13})P_l(\cos\theta_1)\ . \tag{2}$$

Our key simplification is to assume that the functions F_l are separable and symmetric products of functions ϕ_l of each bond length. This leads to the symmetric separable form

$$V_3(r_{12},r_{13},\theta_1)=\sum_l C_l\phi_l(r_{12})\phi_l(r_{13})P_l(\cos\theta_1)\ . \tag{3}$$

Generally, separability is consistent with a local picture for the atomic bonding interactions. This simplification can be motivated by the following physical picture: Atom 2 bonds with atom 1, with a bonding strength that is a function of r_{12}. When an atom 3 is brought near this system, it feels a bonding potential that has azimuthal symmetry and is a function of θ_1. A simple representation of the constrained 1—3 bond is to assume that it has a strength that is a function of r_{13}. Assuming both bonding strength functions to be identical leads to the form (3). It is clear that the physical picture suggested here is not plausible when r_{23} becomes small compared to r_{12} or r_{13} (e.g., at small θ_1). However, the symmetrization in the three-body sum in Eq. (1) restores the proper notion of the primary bonded pair.

The addition theorem for spherical harmonics now reduces the three-body energy to a rotationally invariant scalar product of vectors Φ_{lm} that are simple two-body sums, i.e.,

$$\sum_{2,3} V_3(r_{12},r_{13},\theta_1)=\sum_l C_l\left[\frac{4\pi}{2l+1}\right]\sum_{m=-l}^{l}\Phi_{lm}^{*1}\Phi_{lm}^{1}\ , \tag{4}$$

where

$$\Phi_{lm}^{j}=\sum_2\phi_l(r_{j2})Y_{lm}(\hat{r}_{j2})\ . \tag{5}$$

The Φ_{lm}^{j} vectors are the moments of the structure around atom j that describe its local environment. The calculation of the energy in (1) requires the sum in Eq. (4) to be corrected for the case when indices 2,3 are identical. This introduces a modification of the two-body interaction,

$$\sum_{2,3}{}' V_3(r_{12},r_{13},\theta_1)=\sum_{2,3} V_3(r_{12},r_{13},\theta_1)-\sum_2 f_3(r_{12})\ , \tag{6}$$

where

$$f_3(r)=\sum_l C_l\phi_l^2(r)\ . \tag{7}$$

The classical model presented here is quite general. There exist interesting connections of this classical model to the theory of bond orientational order in liquids and to the embedded atom method for the close-packed metals.

Moments Φ_{lm} very similar to (5), have been developed by Steinhardt, Nelson, and Ronchetti[9] to describe the local bond-orientational order in supercooled liquids. From this viewpoint, the Φ_{lm} vectors are order parameters describing the local bond-orientational order in the solid. The three-body energy (4) can be viewed as the quadratic term in a Landau expansion of the structural energy in terms of this order parameter. This perspective provides a natural way to extend the Landau expansion to a cubic term, involving a contraction of 3 Φ_{lm}'s, that physically represents a four-body interaction. The proper form is[9]

$$E^{(4)}=\sum_l C_l\sum_{m_i}\begin{pmatrix} l & l & l \\ m_1 & m_2 & m_3\end{pmatrix}\Phi_{lm_1}\Phi_{lm_2}\Phi_{lm_3}\ . \tag{8}$$

The m-dependent coefficients are the Wigner $3j$ symbols. These coefficients are nonvanishing only when the sum over the m_i is zero. The form (8) is an invariant under rotations of the real coordinate system. The $l=0$ term of the angular momentum expansion is simply $(\Phi_{00})^3$. Although we have not attempted to fit such four-body terms for Si potentials, these may be useful for other systems.

It is worth noting that the $l=0$ moment Φ_{00} is among the simplest invariants. Φ_{00} describes the local atomic coordination and is proportional to the atomic density. The quantities $(\Phi_{00})^2$ and $(\Phi_{00})^3$ are the simplest three- and four-body interactions, and are independent of bond angles.

It is possible to draw interesting connections between these interatomic potentials and the embedded-atom method developed for structural energies of close-packed metals.[10,11] In the embedded-atom method the structural energy is approximated[10,11] to be

$$E_{\rm tot}=\sum_i F_i(\rho_{h,i})+\tfrac{1}{2}\sum_{i,j}{}' v(R_{ij})\ . \tag{9}$$

Here $\rho_{h,i}$ is the host electron density at atomic i due to the other atoms of the system and $F_i(\rho)$ is the energy to embed atom i in the background electron density ρ. ρ is approximated as a sum of spherical atomic densities. $v(R_{ij})$ is a core-core pair repulsion. The embedding energy is zero for zero electron density and has a negative slope and positive curvature for typical metallic electron

densities. Such forms for the embedding energy have had much success in describing the structural energetics of fcc metals as well as surface reconstruction and defect properties in these systems.[10,11]

We note that an embedding function that varies linearly with the density ρ is equivalent to a purely pairwise interaction. However, an embedding energy that is a quadratic function of the density [Eq. $F(\rho)=C\rho^2$] is equivalent to a separable three-body potential that contains only the product $(\Phi_{00})^2$ in addition to a purely pairwise interaction. The structural energy can be written as

$$E_{\rm tot}=2C\sum_i\sum_j\psi^2(R_{ji})+2C\sum_i\sum_{j,k}{}'\psi(R_{ij})\psi(R_{ki})+\tfrac{1}{2}\sum_{i,j}{}'v(R_{ij})\ . \quad (10)$$

The density here is expressed as

$$\rho(R_i)=\sum_j\psi(R_{ji})\ , \quad (11)$$

a superposition of densities from all atomic sites. Embedding functions that are polynomials of degree higher than quadratic represent higher multiatom terms, and are all of the form $(\Phi_{00})^n$.

III. LOCAL DENSITY FUNCTIONAL CALCULATIONS FOR Si STRUCTURES

A difficult problem in the implementation of any classical model for structural energies is the choice of physically plausible model parameters. Generally, this can be accomplished by fitting the classical model to either experimental data or to accurate quantum-mechanical calculations. We have chosen to fit to a database of accurate quantum-mechanical calculations performed using the local density approximation for the energies of Si structures. The LDA calculations accurately describe experimental phonon dispersions,[2] the bulk modulus of diamond Si (Ref. 2), and pressures for transitions to metallic phases.[2,3] In this section previous calculations for bulk Si phases are summarized. We have extended the Si database with calculations for energies of Si(111) slabs, layered slabs of metallic Si structures, and interstitials that are described here.

The local density functional calculations of Yin and Cohen[2] for bulk Si structures are shown in Fig. 1. This includes energies of tetrahedral diamond and wurtzite, high-pressure β-tin, hcp, and other simple hypothetical structures. Simple hexagonal Si calculations are from Ref. 3. The energies of the complex tetrahedral structure B-8 (BC-8) (Ref. 12) are useful as tests of classical models. The LDA calculations accurately describe the transitions from diamond to β-tin to simple hexagonal to hcp under increasing pressure. The atomic coordination systematically increases in these transitions.

Many of the metallic structures in Fig. 1 may not have low enough energies to be stable in extended form but many of these features should be important in understanding the structure of molten Si and consequently the crystal-liquid interface. These metallic environments

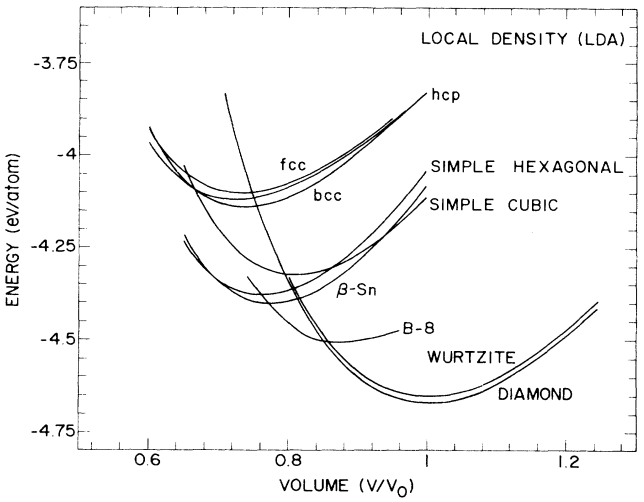

FIG. 1. Energies for simple bulk silicon structures as a function of atomic volume from local density approximation calculations.

can also appear as intermediate states associated with complex dynamical processes. Examples of such processes are the diffusion of a Si self-interstitial and recrystallization processes such as the solid phase growth of a crystalline-amorphous interface.

To account for bond breaking energies we have performed *ab initio* linear augmented-plane-wave (LAPW) calculations[13] for the energies of the partially bonded four-layer and two-layer Si(111) slabs, as a function of the positions of the outermost atomic layers (Figs. 2 and 3). Both calculations describe the tendency of threefold

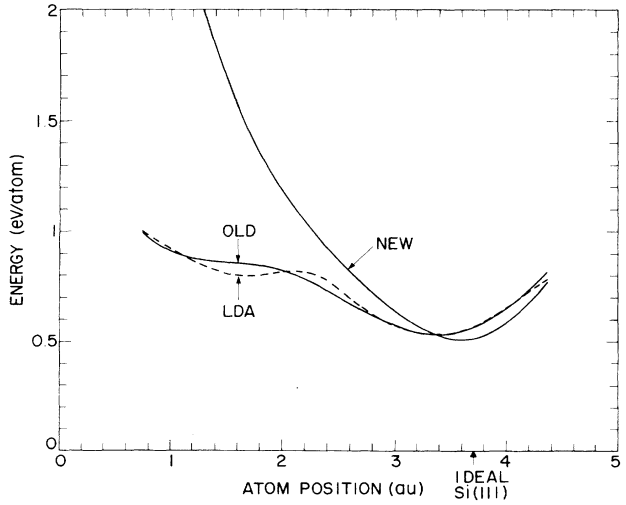

FIG. 2. Energy of a four-layer Si(111) slab from LDA calculations and old and new classical models. The two outermost layers are symmetrically displaced in the normal direction. The distance of either surface layer from the slab center is plotted. At 2.22 Å the slab reduces to two graphitic atomic planes.

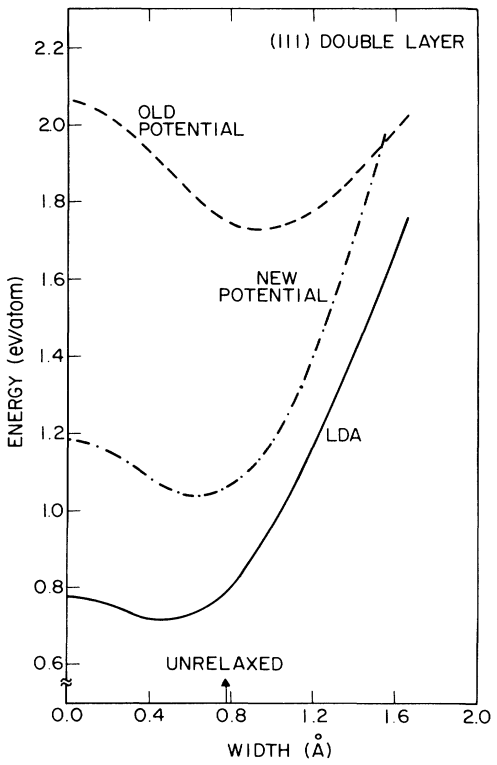

FIG. 3. Energy of a two-layer Si(111) slab [a single (111) double layer] from LDA calculations, compared with predictions for the old and new classical models. Energies of all three curves are relative to the corresponding bulk cohesive energy. Lateral relaxations of the slab were not considered.

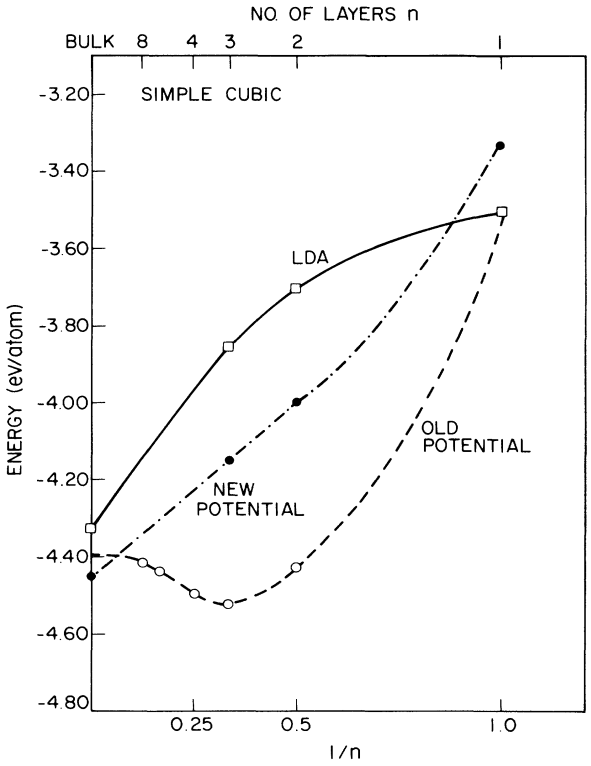

FIG. 4. Energy of n layer simple cubic (100) Si slabs from LDA calculations compared with predictions from old and new classical Si models. The lateral lattice constant was kept fixed at the corresponding bulk equilibrium value. The points represent actual calculations, the curves are drawn for estimation of the surface energies.

coordinated atoms at the surface to become more graphitic and display an energy minimum for a more planar configuration of the surface atoms. The Si(111) surface also shows a similar relaxation. The two-layer slab shows a weak energy variation that was less useful for the fits, but more useful in tests of classical models. The four-layer energy displays a metastable energy minimum caused by a back-bonded configuration when the surface atom is pushed below the second layer and partially bonds to three additional subsurface atoms. Lateral relaxations were not included in either of the slab calculations.

As a further description of surface energies, we have performed LAPW calculations for 1, 2, and 3 layer slabs of simple cubic and simple hexagonal structures as shown in Figs. 4 and 5. We also repeated the bulk calculations for these structures to provide a consistent reference energy. The in-plane lattice constants of the slabs were held fixed at the calculated bulk equilibrium values. Both calculations display positive surface energies which can be approximated by half the slope of the straight-line portions of the energy curves at large layer number.

The balance between the bulk phase energies (Fig. 1) and the surface energies is especially important in determining the equilibrium structures of Si clusters. The simple cubic layers have a surface energy of ~ 0.66 eV per atom. This is lower than the surface energy of a Si(111) slab which is ~ 1.09 eV per atom. The lower surface energies of the metallic environments make it favorable for small Si clusters, that have a large fraction of surface sites, to be metallic and have higher coordination than a microcrystalline structure. The penalty of increased bulk energy is offset by the gain in surface energy for metallic clusters.

We have also performed LAPW calculations for a silicon self-interstitial at the tetrahedral interstitial (T-i) site, using a 9-atom supercell containing the interstitial. We find the T-i to have a formation energy of ~ 4.05 eV that is comparable to the cohesive energy of 4.65 eV. The T-i is then to a large extent nonbonded. The unrelaxed hexagonal interstitial was also found to have an energy similar to the T-i. These results for the T-i energy are consistent with other LDA calculations of interstitials and vacancies in Si.[14,15]

The partially bonded Si(111) slab energies, the positive surface energies of metallic slabs, the large formation energies of self-interstitials, and the bulk-phase energies are the data we have used to construct classical model potentials.

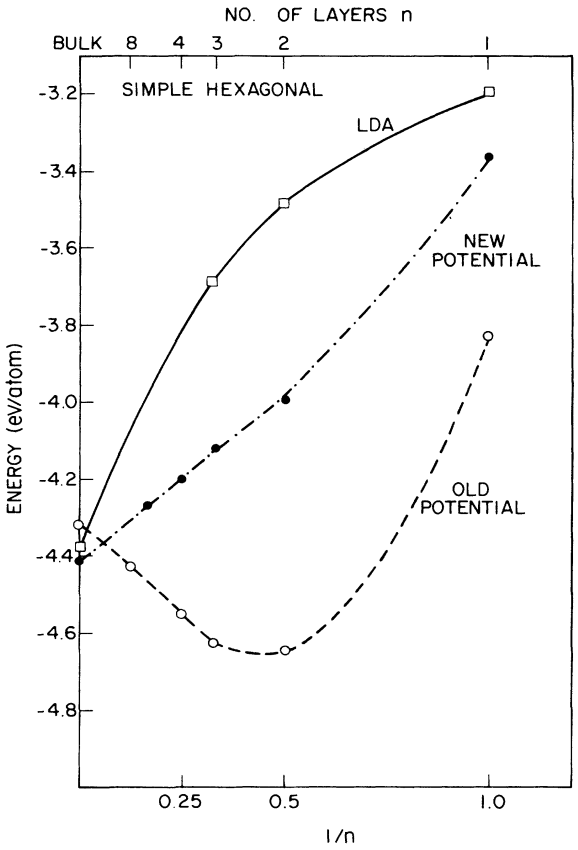

FIG. 5. Energy of n layer simple hexagonal (001) Si slabs from LDA calculations compared with predictions from old and new classical models. The lateral lattice constant was kept fixed at the corresponding bulk equilibrium value.

IV. DEVELOPMENT OF CLASSICAL POTENTIALS FOR SILICON

A. Fitting strategies

We have explored the ability of the classical two and three-body potential models to provide a global fit to the LDA calculations described in Sec. III. These structures span a wide range of atomic coordinations, bond angles, and bond lengths. The expectation is that complex structures will locally resemble one of the fitting structures, and that the classical model will, in effect, interpolate the local density results.

We have examined a few short-range monotonic functional forms for the three-body potential, together with similar forms for the two-body potential. For example, the simple exponential class of functions $\phi_l = e^{-\alpha_l r}$ was used together with the generalized Morse two-body potential

$$V_2(r) = A_1 e^{-\lambda_1 r} + A_2 e^{-\lambda_2 r} . \tag{12}$$

The nonlinear parameters for this model are the decays λ_1, λ_2, and α_l whereas A_1, A_2, and C_l are linear parameters.

Our initial fitting strategy was to treat the coefficients C_l as independent linear parameters. For the least-squares fit to the database energies we minimized the objective function

$$f_{\text{obj}} = \sum_{\nu} \left[E_\nu - \sum_{\mu} B_\mu M_{\mu\nu}(X_\nu) \right]^2 . \tag{13}$$

Here B_μ represents linear parameters (A_i and C_l), E_ν are the database energies, and X_ν represents both the atomic volumes and structures chosen. $M_{\mu\nu}$ is the energy matrix constructed from the two- or three-body potential functions. Minimizing (13) with respect to the linear parameters B_μ results in linear matrix equations

$$\sum_{\nu} M_{\nu\beta} \left[\sum_{\mu} B_\mu M_{\mu\nu} \right] = \sum_{\nu} E_\nu M_{\beta\mu} . \tag{14}$$

The n nonlinear parameters (λ_1, λ_2, and α_l) were varied with a simplex routine which calculates the objective function at the $(n+1)$ vertices of a simplex in the space of the n nonlinear parameters. For each set of nonlinear parameters, Eq. (14) was solved for the values of the linear variables. The points of the simplex were varied to shrink it around a minimum of the objective function.[16] A useful fitting strategy was to limit the number of nonlinear parameters by constraining the higher l components to have the same decay rates.

B. Results of fit: "Old" potential

Our initial approach was to agument the existing database of bulk energies (Fig. 1) with the Si(111) slab energies (Figs. 2 and 3) for fitting the classical model. Studies and tests of the resulting model potential led to the further LDA calculations for the metallic slabs and the *T-i*. Our best initial fit to the LDA calculations of Fig. 1 and the four-layer slab (Fig. 2) were with the family of simple exponential functions [Eq. (12)]. The parameters for this fit are given in Table I. The results of our fit compare very well with the quantum-mechanical energies for Si(111) slab, as shown in Fig. 2. Our global fit to the crystal structures shown in Fig. 6, agrees with the quantum-mechanical results of Fig. 1 to within an rms error of 0.05 eV and displays the correct structural trends over a large range of atomic volumes. The first high-pressure phase is correctly predicted to be β-tin.

TABLE I. The values of the parameters for the old two- and three-body potentials. λ_l and α_1, α_2 are nonlinear decay parameters; C_l and A_1, A_2 are the linear coefficients.

	l,i	α_i, λ_l (Å^{-1})	$A_i C_l$ (eV)
Two body	1	3.946 668	$0.268\,293\,6 \times 10^5$
	2	1.191 187	$-0.425\,986\,3 \times 10^2$
Three body	0	1.246 156	$0.913\,977\,5 \times 10^2$
	1	1.901 049	$0.164\,401\,3 \times 10^5$
	2	1.786 959	$0.958\,029\,9 \times 10^4$
	3	1.786 959	$0.666\,314\,7 \times 10^4$
	4	1.786 959	$0.398\,771\,0 \times 10^4$
	5	1.786 959	$0.204\,672\,2 \times 10^4$
	6	1.786 959	$0.701\,886\,7 \times 10^3$

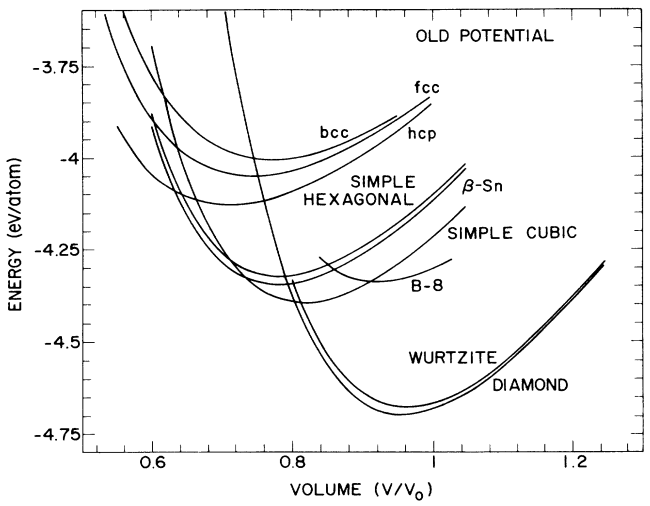

FIG. 6. Predicted energies for bulk silicon structures as a function of the atomic volume from the old classical model. The energy curves compare very well with the quantum-mechanical results of Fig. 1.

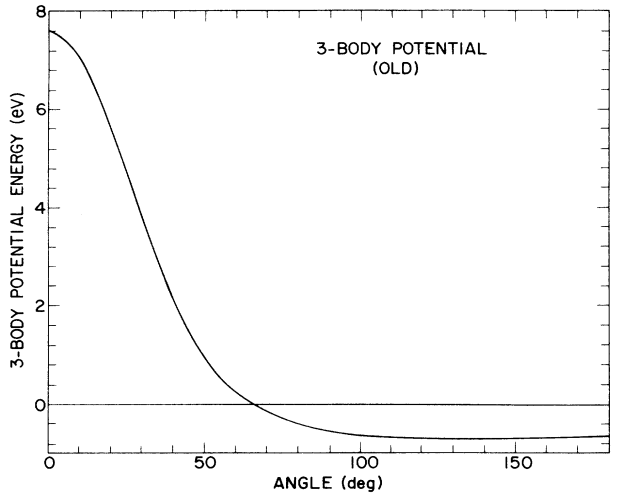

FIG. 7. Angular variation of the three-body potential for the old classical model. The two bond lengths were kept fixed at the equilibrium diamond-Si bond length (2.35 Å).

The structural energies display three structural groupings similar to the LDA results. In Fig. 6, bcc, simple (Si)-hexagonal, and B-8 were test structures that were not fitted. Si hexagonal is very close to β-tin as it should be. bcc is also modeled well.

Wurtzite is higher energy than diamond-Si. hcp is not as well fitted as other phases and s cubic is somewhat lower in energy than the quantum-mechanical result. B-8 is too high in energy, indicating that this model is too stiff for local distortions around the diamond structure. Our diamond Si phase has an equilibrium bond length of 2.32 Å (experimentally 2.351 Å), but the nonlinear decay parameters could be uniformly scaled to produce the experimental bulk bond length if desired.

The resulting three-body potential exhibits a weak angular dependence for $90° \lesssim \theta \lesssim 180°$ with a shallow minimum around $\theta \approx 110°-115°$, and is plotted in Fig. 7 for the diamond bond length. Bond angles of $\theta < 70°$ generate strong repulsions. The two-body potential, labeled old in Fig. 8, has a minimum value of 1.09 eV at the minimum positions of 2.77 Å.

These potentials were tested with molecular dynamics simulations on complex structures. The atomic forces can be analytically derived from the energy expressions and have been presented previously.[4] Using the atomic forces, a Langevin molecular-dynamics scheme was developed in which the Si atoms are immersed in a viscous medium and the dynamics is controlled by the internal atomic forces together with a random fluctuating force from the heat bath.[17].

The molecular-dynamics simulations revealed symptoms of two deficiencies of this classical model. First, an interstitial-vacancy pair was created in a 64-atom supercell of the diamond structure. Simulated annealing of this configuration did not lead back to the ideal crystal, but resulted in a metastable interstitial site with energy ~ 1.2 eV interstitial above the ideal crystal. At this metastable configuration this interstitial had six partial bonds, and a position between the T-i and the ideal crystal site.

Atomic Si clusters were also examined, and we found metallic coordinations (simple cubic and fcc fragments) to be favored over bulklike tetrahedral coordination (by $\sim 0.2-0.3$ eV per atom) for clusters as large as 256 and 384 atoms.

These molecular-dynamics studies led to further tests. We first found that the classical potential did not test well on the class of multilayer slabs of other bulk struc-

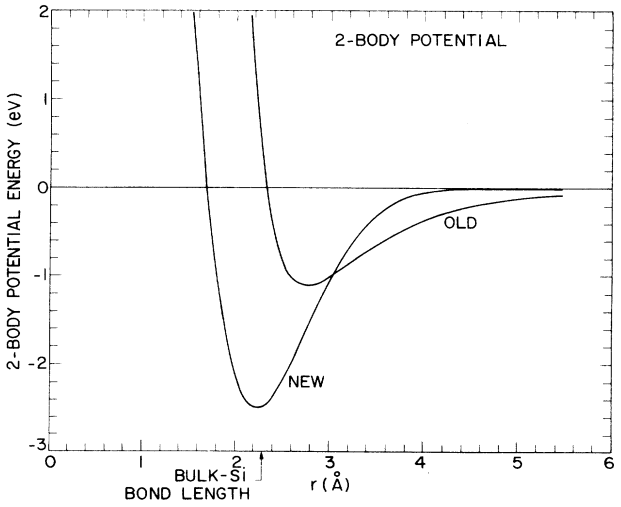

FIG. 8. Comparison of the two-body potentials for the old and new classical Si models. The new model has a deep pair potential with a minimum just inside the bulk Si bond length. The old model pair potential is much weaker and longer ranged.

tures, showing negative surface energies for simple cubic and simple hexagonal layers (Figs. 3 and 4). The negative surface energies artificially favor metallic coordinations for clusters which have a large fraction of surface sites, which is the case for 256 and 384 atom clusters. fcc(100) and fcc(111) slabs also display similar qualitative behavior as shown in Figs. 3 and 4. Although not shown in Fig. 4, the two-layer Si-hexagonal slab laterally relaxes to an energy below the bulk diamond Si structure.

The old potential provided satisfactory formation energies for vacancies (4.8 eV unrelaxed and 4.3 eV relaxed), with the atoms relaxing outward from the vacancy, similar to the relaxation of Si(111) surface atoms. Self-interstitials, however, were described unphysically in the old model—see Table II. The hexagonal self-interstitial had a satisfactory unrelaxed energy but relaxed to a low value (~ 1.2 eV). The tetrahedral interstitial (*T-i*) had an unphysically low unrelaxed energy (~ 0.7 eV) and became more stable than diamond when relaxed (~ -0.33 eV).

The *T-i* is unstable because creating a relaxed *T-i* leads to a large decrease of the two-body energy (-7.76 eV), which is not compensated by the increase of the three-body part (7.43 eV). These energies are relative to adding the extra atom in a perfectly bonded diamond crystal site. The bond-bending repulsion on the four neighbors of the interstitial is clearly not strong enough. This suggests that a somewhat different balance of the two and three-body energies would be more suitable. The bond-breaking energies of the Si(111) slab as well as the *T-i* formation energy suggest a shorter range potential where the three-body potential is dominated by the first two neighbor shells, rather than the 8–10-Å range of the old potential.

C. Explorations of classical models

In an effort to improve on deficiencies of the old model, we have explored alternative classical model potentials by augmenting the previously used database with our LDA calculations of 1, 2, and 3 layer slabs of simple cubic and simple hexagonal, and for the *T-i* energy.

Initially, we first found that adding the layer energies (Figs. 3 and 4) to the database adiabatically altered the parameters of the old potential, making both two- and three-body functions less sharply varying than previously, i.e., the exponential decays are smaller. A Fermi-like function with a cutoff of 5.50 Å and width 0.40 Å could also be incorporated into the model, illustrating the redundancy of the longer-range contributions. The refitted potential displayed satisfactory positive surface energies for the metallic slabs, and similar results for the bulk structures and Si(111) slab as the old potential but did not raise the energy of the *T-i* adequately.

TABLE II. Energies of vacancies and interstitials.

	Energies (eV)			
	Old model		New model	
	Unrelaxed	Relaxed	Unrelaxed	Relaxed
Vacancy	4.803	4.266	3.828	3.828
T interstitial	0.699	≈ -0.33	4.989	3.612
H interstitial	4.905	1.278	9.469	5.090

The energy of a 9-atom supercell containing the *T-i* was then added to the database. We found that to model the *T-i* energy required much shorter-range functions, with parameter values very different from the old potential. It was not possible to fit the *T-i* and all the metallic structures simultaneously. Typically, we used diamond, β-tin, *s*-cubic, the (111) four-layer slab, metallic layers, and the *T-i* in the fitting database. The *T-i* was roughly weighted as much as diamond, while the metallic phases were given a weight of $\approx 25\%$ of diamond. Exponential as well as Gaussian decaying functional forms were examined. Fitting strategies consisted of initially dealing with a few nonlinear parameters by imposing constraints, e.g., having a Morse form for the two-body potential, or having the same decay rates for all l's in the three-body functions. If a stable and unique minimum for the fits was reached, the constraints were gradually relaxed using the values of the variables at the new minimum as the starting point for further fits.

A class of potentials that modeled the *T-i* energy well had short-range exponential functions $e^{-\lambda r}$ with $\lambda \approx 2.7-3.4$. The resulting two-body potential had a minimum at the diamond—Si bond length, with a depth of ~ 3.0 eV. The three-body potential exhibited a slightly oscillatory angular form for angles $60° \leq \theta \leq 150°$, with strong and weak repulsions for $\theta \simeq 0°$ and $\theta = 180°$, respectively. The bulk phases were fit less well. Although β-tin was the lowest energy metallic phase, the close-packed structures were too high in energy. Wurtzite was modeled well. The metallic slabs had positive surface energies, although the interpolation to the bulk was not smooth. The *T-i* has effectively ten neighbors (four at 2.35 Å and six at 2.715 Å), that generate bond angles ranging from 35.3° to 180°. The repulsive three-body energy at small bond angles stabilized the *T-i* to be ~ 3 eV above diamond.

A deficiency of the derived potential was an unphysical energy lowering for metallic structures (β-tin, *s*-cubic) for compressed volumes with nearest-neighbor distances in the range of 2–2.25 Å. Although all the C_l coefficients were positive, this behavior was due to the negative $l \neq 0$ piece of the three-body energy for these structures, that increased in magnitude more rapidly than the repulsive $l = 0$ part. We found that the collapse problem could be averted by saturating the three-body potential at a bond length of ~ 2.25 Å. The resulting model, however, displayed an unphysical stiffening of the diamond-Si energy curve at volumes just smaller than the equilibrium value and almost zero formation energy for the hexagonal interstitial.

Another approach that we examined was to use a combination of short- and long-range functions. This was motivated by the observation that tetrahedral properties, such as the *T-i* formation energy or the cohesive energies of Si(111) slabs, can be estimated from local bond counting arguments. However, an accurate description of the metallic phases required the old poten-

TABLE III. rms energy errors for the best fits of classical models with short- and long-range radial functions $\exp[-(r/r_1)^m]$, $\exp[-(r/r_2)^m]$ for the three-body part. Corresponding functions $\exp[-(r/r_1)^m]$ and $\exp[-n(r/r_1)^m]$ were used for the attractive and repulsive two-body potential. m characterizes the family of radial functions, whereas n characterizes the two-body potential.

m \ n	2	3	4
1	0.070	0.077	0.085
2	0.051	0.065	0.081
3	0.055	0.050	0.057
4	0.055	0.044	0.050
5		0.046	
6		0.134	

tial to be long ranged.

We examined functional forms of $e^{-\alpha r^m}$ and $e^{-\beta r^m}$ for the short- and long-range three-body functions with angular momentum components up to $l=4$. The radial functions $e^{-\alpha r^m}$ and $e^{-n\alpha r^m}$ were used for the attractive and repulsive two-body potential, values of m and n were varied with n typically between 2 and 4. Constraining the attractive two-body potential to have the same decay as the longer-ranged three-body part is, in spirit, similar to Tersoff's ansatz that the effective two-body potential becomes weaker with increasing coordination.[8]

For chosen values of n and m, the model had two nonlinear parameters α,β and the fitting resulted in unique minima. The rms error of the fits are displayed in Table III together with the values of the effective ranges $r_1=\alpha^{1/m}$ and $r_2=\beta^{1/m}$ in Table IV. Both bulk and slab energies were modeled well with rms errors of 0.04–0.06 eV. However, the $l=0$ part of one or both of the three-body potentials were often negative. This is contrary to the physical picture of a repulsive $l=0$ interaction that increases for the higher coordinated structures, and balances the increased attraction of the two-body energy. The three-body energy was attractive for both diamond and the Si(111) four-layer slab, and was responsible for equilibrium of both these structures. Potential models with these properties were judged to be mathematically well defined, but physically implausible. Explorations of such classical models may be an aspect of this problem for further study.

TABLE IV. Values of r_1 and r_2 (in Å) for optimized classical models with two radial functions $\exp[-(r/r_1)^m]$ and $\exp[-(r/r_2)^m]$. n characterizes the two-body part (see Table III caption). Each member of the family of potentials is characterized by the two nonlinear parameters n and m.

m \ n	2		3		4	
1	0.70	0.91	0.68	1.10	0.60	1.33
2	1.95	0.46	1.87	1.26	1.81	1.07
3	2.37	1.00	2.30	1.03	2.31	1.03
4	2.51	1.00	2.57	1.03	2.61	1.05
5			2.71	1.03		
6			2.09	1.10		

D. New Si-potential

A large part of the problems encountered with exploration of classical models arose from the ability of the three-body potential energy to be attractive, and to become unphysically large and attractive for certain configurations. Even if all linear coefficients C_l are positive, the three-body energy [Eq. (3)] need not necessarily be always repulsive.

An obvious solution is to make the ansatz that the three-body energy should be purely repulsive, so that cohesion is caused by the two-body potential. This ansatz need not be true if terms higher than three-body are included in the structural energy expansion. With a view to globally stabilizing the diamond structure, we examined constrained forms of the three-body potential that had a minimum at the tetrahedral angle.

Physically appealing fits were obtained with the three-body potential

$$V_3(r_{12},r_{13},\theta)=[B_1\psi_1(r_{12})\psi_1(r_{13})(\cos\theta+\tfrac{1}{3})^2 + B_2\psi_2(r_{12})\psi_2(r_{13})(\cos\theta+\tfrac{1}{3})^3] \times f_c(r_{12})f_c(r_{13}) . \quad (15)$$

This is a generalization of the separable form (3) to two classes of radial functions. The angular variation in (13) is a special case of the expansion in Lengendre polynomials where the coefficients are constrained to be $C_0=(\frac{4}{9})B_1$; $C_1=C_2=(\frac{2}{3})B_1$, for the Keating-type $(\cos\theta+\frac{1}{3})^2$ part; and $C_0'=0.370\,370B_2$, $C_1'=0.9333B_2$, $C_2'=(\frac{2}{3})B_2$, $C_3'=(\frac{2}{5})B_2$, for the $(\cos\theta+\frac{1}{3})^3$ term. Our best fits were obtained with Gaussian functions $\psi_i=e^{-\alpha_i r^2}$, together with the two-body potential

$$V_2(r)=(A_1e^{-\lambda_1 r^2}+A_2e^{-\lambda_2 r^2})f_c(r) , \quad (16)$$

and the cutoff function

$$f_c(r)=\{1+\exp[(r-r_c)/\mu]\}^{-1} . \quad (17)$$

Parameters for the new potential are shown in Table V. This potential contains many fewer parameters (eight or ten including the cutoff function), than the old poten-

TABLE V. Parameters for new potential model.

i	λ_1 (Å^{-2})	A_i (eV)
1	0.520 083 6	$0.142\,292\,2\times10^3$
2	0.420 693 1	$-0.107\,033\,8\times10^3$
	α_i (Å^{-2})	B_i (eV)
1	0.303 437 3	$0.130\,299\,0\times10^2$
2	0.319 190 3	0.672 073 9
r_c	3.952 735 7 Å	
μ	0.312 058 0 Å	

tial. As in previous explorations, we initially started with two nonlinear parameters—one describing a constrained two-body potential, and a $(\cos\theta+\frac{1}{3})^2$ angular three-body term. Variational flexibility was increased in the two-body part and by adding the $(\cos\theta+\frac{1}{3})^3$ angular term. This potential was not sensitive to the parameters chosen for the cutoff function. The nonlinear parameters were scaled for the equilibrium of diamond-Si to be at the experimental value. Adding a further angular variation term $(\cos\theta+\frac{1}{3})^4$ tended to be redundant. Allowing the exponent ν in the radial functions $e^{-\alpha_i r^\nu}$; $e^{-\lambda_i r^\nu}$ to vary produced very similar potentials for ν in the range 2–2.20.

A success of the "new" Si potential is that it models the formation energies of interstitials and vacancies well (see Table II). The unrelaxed and relaxed energies are 4.9 and 3.6 eV for the *T-i*, and 9.5 and 5.1 eV for the *H-i*. The *T-i* effectively has ten near neighbors and the very nontetrahedral bond angles (35.2°, 180°, etc.) generate large repulsions.

Tests of the new potential were made on the slab structures (Figs. 2–5). The new potential has positive surface energies for metallic slabs (Figs. 4 and 5) and agrees much better with the LDA results for the slabs than the old potential. The new potential models the bond-breaking energy well. The value of the energy of the Si(111) four-layer slab is very close to the LDA result (Fig. 2), although it is somewhat stiffer for distortions of the outermost layer that compress the surface bonds. The energy variation of the Si(111) slab is very similar in form to the LDA result (Fig. 3), and the absolute energy of the slab is about ≈ 0.2 eV higher than the LDA result. In comparison, for the old potential, the two-layer slab loses almost half of the bulk cohesive energy, due to the loss of neighbors for the long-ranged model. The (111) slabs were not used in the fit for the new potential.

As a necessary compromise, the bulk structures are much less accurately fit than with the previous potential.

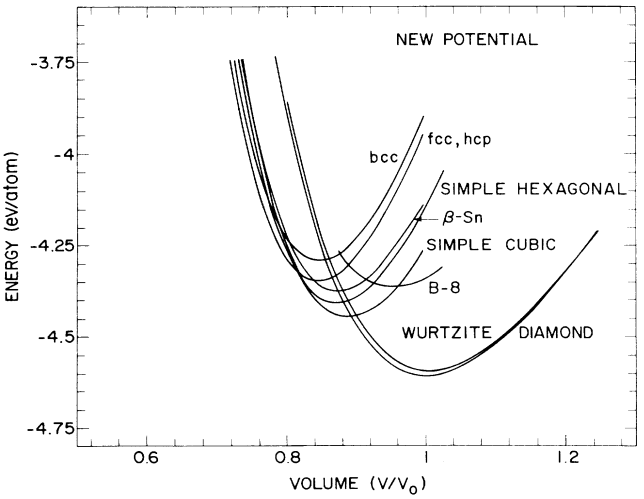

FIG. 9. Energies for bulk Si phases from the new classical potential.

Physically plausible trends are obtained though for the energy of the closer packed structures (Fig. 9). Diamond-Si would be predicted to make a transition under pressure to a six-coordinated structure (simple cubic). Energy differences between diamond and the metallic structures are smaller than in the LDA, and all phases have somewhat higher bulk moduli than the LDA results. Wurtzite is higher energy than diamond by ≈ 0.02 eV.

While our models have not been developed to reproduce the energies of small distortions around the diamond structure, it is of interest for some applications to have a quantitative measure of their performance in this respect. Although it is possible to calculate a full dynamical matrix for these potentials, we confined our investigation to the numerical evaluation of the curvature of the energy surface for a few high-symmetry phonon distortions. The results are shown in Table VI for the old and new models, LDA,[18] and experiment.[19] The four modes considered are longitudinal-transverse optic at Γ, the degenerate longitudinal optic and acoustic at X, the transverse optic at X, and the transverse acoustic at X. As noted in Sec. IV B, the old model is considerably too stiff, particularly for the optic models. The new model, however, is remarkably good, especially considering that no small-distortion results entered the fit. This suggest that the new model should give a reasonable account of the thermal properties and melting of Si.

The angular form of the new three-body potential is similar to the Keating form and the Stillinger-Weber model potential,[7] and is shown in Fig. 10. Although small in strength, the $(\cos\theta+\frac{1}{3})^3$ provides additional variational freedom for the angular function. The new two-body potential (Fig. 8) is consistent with the properties of the Si_2 molecule. It would predict the Si_2 bond length to be ~ 2.34 A, somewhat smaller than the diamond-Si bond length (2.35 Å), with an energy of ~ 2.5 eV, which is more strongly bound than half the cohesive energy of diamond-Si. The new two-body potential is stiffer, around the minimum, than the bond-stretching Keating potential. The angular variation of the new potential around the tetrahedral angle (Fig. 10) is much softer than the Keating model.[1]

With a view to studying the global stability of the diamond structure, we performed a few simple molecular dynamics simulations of the new model on 8-atom supercells of diamond-Si and found satisfactory results. We found that a vacancy $-T$-*i* pair relaxed to the crystal

TABLE VI. Comparison of Si phonon frequencies (in THz) calculated from our old and new models with LDA (Ref. 18) and experimental (Ref. 19) values.

	LTO (Γ)	LOA (X)	TO (X)	TA (X)
Old	24.3	15.6	24.8	7.2
New	16.0	12.2	14.5	5.6
LDA	15.2	12.2	13.5	4.5
Expt.	15.5	12.3	13.9	4.5

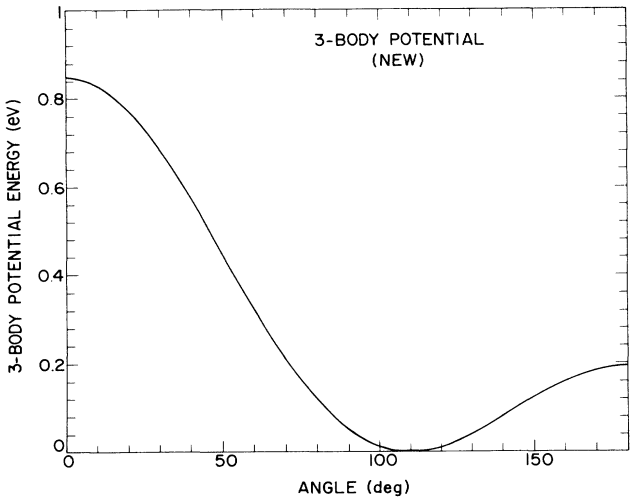

FIG. 10. Angular variation of the three-body potential for the new classical Si model. The two bond lengths were fixed at the equilibrium Si bond length (2.35 Å).

ground state. Simulated annealing of the diamond structure led back to diamond when cooled.

V. MINIMUM ENERGY STRUCTURES OF Si-ATOM CLUSTERS

We have investigated minimum energy structures for Si-atom clusters using both the new and old potentials. These calculations were performed with a view to calibrating the classical models against recent quantum-mechanical calculations for N atom Si clusters ($N=3-10$).[20,21] These calibrations are especially important for estimating the accuracy, and feasibility, of further investigations of the structures of large clusters with the classical models. We have extensively discussed in this paper the applicability of the classical models for extended structures. Here we examine the opposite extreme of small clusters.

Energy minima were found with a combination of steepest descents and simulated annealing methods[17,22] within the Langevin molecular-dynamics approach. For the small clusters, there are only a few minima, and we are confident that our methods found the absolute minimum for each. With the old classical model we generally found compact symmetric structures to have the lowest energies. These structures had the maximum number of bonds for a given number of atoms. The octahedron and decahedron were more stable than the 6-atom chair and 10-atom adamantane cage fragments of the diamond structure (see Table VI). Generally the structures were dominated by the two-body potential. Bond-bending distortions and bond angles that were very different from tetrahedral, were energetically less expensive. The clusters are more weakly bound than in quantum-mechanical calculations, since a sizable fraction of the cohesion is lost with the reduced number of neighbors. Bond lengths for the optimized geometries varied between 2.60–2.75 Å, a feature that resulted from the minimum of the two-body potential at 2.77 Å.

The new potential produced somewhat different optimized configurations (Table VI). Generally, the stronger and shorter-ranged three-body potential led to more sever energy penalties for structures with bond angles that were much different from tetrahedral. For the trimer, an isosceles triangle with an apex angle of 79° and two bond lengths of 2.29 Å (shorter than the 2.35-Å bulk diamond bond) had the lowest energy. This, in fact, agrees well with the quantum-mechanical results[20] of 77° and 2.23 Å for the apex angle and bond lengths of the trimer.

For both 4- and 5-atom clusters planar configurations were preferred. These were the square (with bond length 2.34 Å) and the pentagon with 2.29 Å bonds and 108° bond angles. Symmetry-reducing distortions of the square were not energetically favored. The nearly tetrahedral bond angles of the pentagon favored it over more compact structures (pyramid, bipyramid) that have more bonds (see Table VI).

For 6 atoms the new potential favors an asymmetric structure in which 4 atoms have three bonds and the other two have two bonds, with eight bonds in the structure with bond lengths 2.37 and 2.45 Å. This is topologically equivalent to the optimized structure obtained by Raghavachari.[20] Although the symmetric octahedron has more bonds (12) than this optimized structure, the bonds of the octahedron are weaker (2.62 Å) to compensate for the larger three-body repulsions from non-tetrahedral bond angles. The chair-fragment of the diamond structure was significantly higher in energy.

For 10 atoms we find the decahedron to be the lowest energy structure. The decahedron can be formed by a relative rotation of the two opposite faces of a cube by 45°, followed by adding two capping atoms to these faces. Bond lengths within the cube were 2.47 and 2.92 Å (for the square subunits) and 2.49 Å for the capping adatoms. The decahedron is also more stable than the adamantine cage fragment of the diamond structure. Other metastable minima found for 10 atoms are listed in Table VII.

We note that the minimum energy structures for 3, 4, and 6 atoms are similar to the quantum-mechanical results, although there are clearly differences for 5 and 10 atoms. A significant difference is that the four-capped octahedron is not energetically favored with the classical models, although it is the lowest energy structure found from *ab initio* methods for 10 atoms. Although the bonds inside the octahedron are weaker (2.86 Å) than those of the adatom caps (2.48 Å), the large bond angle distortions do not favor this structure. Quantum-mechanical calculations[20,21] indicate a greater flexibility for the bonding to deviate from a tetrahedral environment than the new classical model. Generally, electronic effects such as π bonding became increasingly important for small clusters. Such effects are difficult to describe with a purely classical model.

With a view to studying the structures of larger Si clusters with classical models, we found energy minima of 32-atom clusters for both classical models with simu-

TABLE VII. Energy minima of N-atom silicon clusters with new and old potentials. The first structure for each N is the minimum-energy structure with the new potential. For $N=3-5$ only the minimum-energy structure with the old potential is listed.

N	Structure	Energy eV/atom New potential	Energy eV/atom Old potential
3	Isosceles triangle	−1.70	
	Equilateral triangle		−0.97
4	Square	−2.28	
	Pyramid	−2.10	−1.31
5	Pentagon	−2.50	
	Pyramid	−2.44	−1.58
	Bipyramid	−2.43	
	Tetrahedron	−2.06	
6	Assymetric structure	−2.70	
	Octahedron	−2.64	−1.85
	Chair (diamond fragment)	−2.55	−1.43
10	Decahedron (twisted cube + two caps)	−3.35	−2.56
	Cube + two caps	−3.20	−2.45
	Adamanatine Cage	−3.08	−2.34
	Octahedron + four caps	−2.92	−2.29
	Body-centered cube + cap		−2.49

lated annealing. For these larger clusters, there are many nearly equivalent minima, and our annealing runs almost certainly did not find the absolute minimum.[17] Typical annealed configurations are shown in Fig. 11 for the old potential and Fig. 12 for the new potential. The differences between the two classical models is visually evident from these figures. The old potential led to strongly metallic clusters with an average coordination of ≈ 7, which internal atoms having 8–9 bonds and surface atoms with 4–6 bonds. A shell-like structure around the center of the cluster is present (see Fig. 11). On the other hand, the new model generated only weakly metallic 32-atom clusters that were more open (i.e., less dense). Some of the interior atoms had 6 bonds, although most of the surface atoms had 3–4 bonds. The resulting configuration has the appearance of a disor-

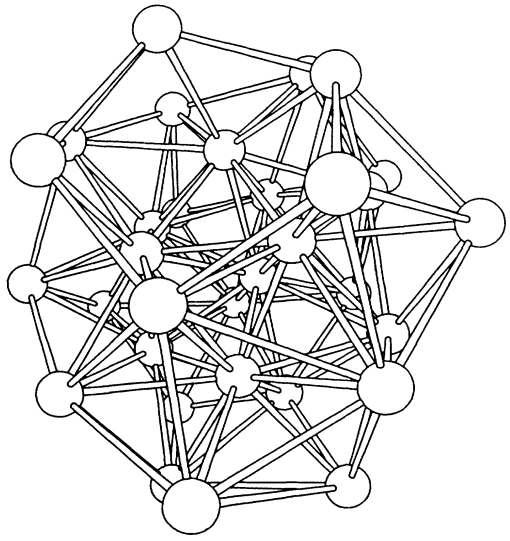

FIG. 11. Structure of an annealed low-energy state for a 32 atom Si cluster, modeled with the old Si potential. The cluster is strongly metallic with an average coordination of ≈ 9. Bonds have been drawn for all atom pairs within the first peak of the pair distribution function (<3.3 Å).

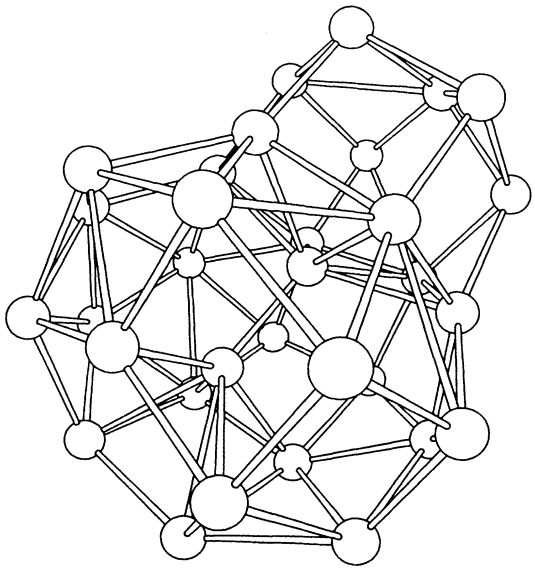

FIG. 12. Structure of an annealed low-energy state of a 32 atom Si cluster with the new potential. Bonds have been drawn for all atom pairs that lie within the first peak of the pair distribution function (<3.1 Å).

dered fragment.

While the small 3-10 atom Si clusters are clearly strongly reconstructed with bonding very different from the bulk, there must be a crossover to a microcrystalline structure with increasing cluster size. We have made a qualitative estimate of the cluster size required for this crossover by comparing energies of an octahedron that has diamond-like interior atoms and (111) faces, and a metallic cube where the interior atoms have sixfold coordination. The energies of the surface atoms were approximated by the surface energies from our LDA calculations (Figs. 3 and 4) for diamond and (100) s-cubic slabs of -3.58 and -3.64 eV, whereas bulk energies were simply those of the bulk phases. This approximation neglects energies of edge atoms and is justified only for large clusters. With the LDA energies we find the diamondlike octahedron to be favored over the cube for clusters larger than ~ 300 atoms. The lower surface energies of the simple cubic structure favor it at small cluster sizes.

We have made the same estimate of the crossover with the new model that yielded positive surface energies. We find the diamondlike octahedron to be preferred only for N above ~ 5000 atoms. This estimate is unrealistically high due to the low energy difference ΔE of 0.15 eV between the diamond and s-cubic bulk phases, compared to the LDA result of 0.28 eV. The crossover size N varies as $(\Delta E)^{-3}$, indicating the sensitivity to details of the classical model.

VI. SUMMARY AND CONCLUSIONS

An important ansatz in the present work is the restriction to two- and three-body models. This restriction was imposed to make the derivation of atomic forces tractable and consequently molecular dynamics feasible. However, it is not *a priori* obvious whether or not four-body or higher multibody contributions are large for covalent semiconductors. One direction for improvement of the present classical models would be a selective inclusion of some higher-body terms. Clearly the present classical models need improvement in being able to provide a more satisfactory global fit to quantum-mechanical energies for a range of structures.

We caution that electronic effects are outside the scope of any classical model. An example of such an effect is the diffusion of self-interstitials in Si. The rapid diffusivity, particularly under electron irradiation conditions, is believed to be due to absorption and emission of electrons from the interstitial connected with the motion of defect electronic levels in the gap.[14,15] Such diffusion cannot be described classically. A similar difficulty for the present classical models is the need to model both sp^3 and s^2p^2 electronic configurations, as well as configurations intermediate these two limits.

In summary, we have developed a general theory for two- and three-body classical interatomic potentials for describing the structural energy of a solid. We have explored the ability of these classical models to model a range of quantum-mechanical calculations for bulk, surface, and clusters of silicon. We have derived two different potentials—one describes very well high-pressure properties of Si and simple surface energies. The deficiencies of this model for interstitial and layered structures were improved upon and led to a new classical model that is more appropriate for properties of the tetrahedral structure, at the expense of describing non-tetrahedral configurations poorer. We expect that the new potential will be useful in molecular-dynamics simulations of amorphous-Si structures and crystal growth processes such as molecular beam epitaxy or the solid phase epitaxial growth of a crystal amorphous interface. Finally, we believe that the discussion of the intermediate stages in the development of these fits will serve as a useful guide to those undertaking similar research for another material, or requiring a different set of criteria to be satisfied for Si.

---

*Present address: Microelectronics Research Center, Iowa State University, 1925 School Road, Ames, IA 50011.

[1]P. N. Keating, Phys. Rev. **145**, 637 (1966).
[2]M. T. Yin and M. L. Cohen, Phys. Rev. B **26**, 5668 (1982); Phys. Rev. Lett. **45**, 1004 (1980).
[3]R. Needs and R. M. Martin, Phys. Rev. B **230**, 5372 (1984); K. J. Chang and M. L. Cohen, *ibid.* **30**, 5376 (1984).
[4]R. Biswas and D. R. Hamann, Phys. Rev. Lett. **55**, 2001 (1985).
[5]E. Pearson, T. Takai, T. Halicioglu, and W. A. Tiller, J. Cryst. Growth **70**, 33 (1984); T. Takai, T. Halicioglu, and W. A. Tiller, Scr. Metal. **19**, 709 (1985).
[6]B. M. Axilrod and E. Teller, J. Chem. Phys. **11**, 299 (1943).
[7]F. Stillinger and T. Weber, Phys. Rev. B **31**, 5262 (1985).
[8]J. Tersoff, Phys. Rev. Lett. **56**, 632 (1986).
[9]P. Steinhardt, D. Nelson, and M. Ronchetti, Phys. Rev. B **28**, 784 (1983).
[10]M. S. Daw and M. I. Baskes, Phys. Rev. Lett. **50**, 1285 (1983).
[11]S. M. Foiles, M. I. Baskes, and M. S. Daw, Phys. Rev. B **33**, 7983 (1986).
[12]R. Biswas, R. M. Martin, R. J. Needs, and O. H. Nielsen, Phys. Rev. B **30**, 3010 (1984).
[13]L. F. Mattheiss and D. R. Hamann, Phys. Rev. B **33**, 823 (1986).
[14]G. A. Baraff and M. Schlüter, Phys. Rev. B **30**, 3460 (1984).
[15]Y. Bar-Yam and J. D. Joannopoulos, Phys. Rev. Lett. **52**, 1129 (1984).
[16]J. A. Nelder and R. Mead, Comput. J. **7**, 308 (1965).
[17]R. Biswas and D. R. Hamann, Phys. Rev. B **34**, 895 (1986).
[18]M. T. Yin and M. L. Cohen, Phys. Rev. B **26**, 3259 (1982).
[19]G. Dolling, *Inelastic Scattering of Neutrons in Solids and Liquids* (IAEA, Vienna, 1963), Vol. II, p. 37; G. Nilsson and G. Nelin, Phys. Rev. B **6**, 3777 (1972).
[20]K. Raghavachari and V. Logovinsky, Phys. Rev. Lett. **55**, 2853 (1985).
[21]D. Tomanek and M. Schlüter, Phys. Rev. Lett. **56**, 1055 (1986).
[22]S. Kirkpatrick, C. D. Gelatt, and M. P. Vecchi, Science **20**, 671 (1983).